ISBN: 978-3-95450-253-0 ISSN: 2673-5571 doi:10.18429/JACoW-HB2023-TUC2I2

SNS LINAC BEAM DYNAMICS: WHAT WE UNDERSTAND, AND WHAT WE DON'T*

A.P. Shishlo†, SNS, Oak Ridge National Laboratory, Oak Ridge, TN, USA

Abstract

The Spallation Neutron Source (SNS) linac accelerates H^- ions to 1.05 GeV before injecting them into the ring. The beam power on the target is 1.7 MW. The linac includes three main parts: a front-end with an ion source, radiofrequency quadrupole (RFQ), and Medium Energy Beam Transport (MEBT) section; a room temperature linac with Drift Tube Linac (DTL) and Coupled Cavity Linac (CCL) sections; and a superconducting linac (SCL). The linac has been operating since 2005. This talk discusses the beam diagnostics and simulation models used in the linac tuning and beam loss reduction efforts over the past 18 years. Considerations about future beam physics experiments and simulation software improvements are outlined.

INTRODUCTION

The Spallation Neutron Source (SNS) accelerator includes a pulsed linac which accelerates negative hydrogen ions to 1.05 GeV, a storage ring that accumulates a proton beam for 1 ms, and beam transport lines that deliver ions to the ring and protons to a liquid mercury target [1]. These protons produce neutrons in spallation reactions. The Spallation Neutron Source is a user facility that provides a reliable and predictable high-density flux of neutrons to 19 instrument stations. The minimal 90% availability goal during the scheduled production time demands an efficient operation of the complex SNS facility. An important contribution to these efforts was acquiring an empirical and model-based knowledge of the beam dynamics in the linac.

During the early stage of SNS commissioning, there was a hope to set the operational parameters of the SNS linac to their design values using computer simulation models and the available diagnostic tools. It did not happen. The biggest problem was unexpected beam loss in the superconducting section of the linac [2]. Later, it was found that the source of beam loss in the SCL was the intra-beam stripping (IBSt) mechanism [3]. This problem was solved before it was explained. The beam loss was reduced empirically by reducing the transverse focusing by 40% [2]. Since then, empirical beam loss reduction in the linac and other parts of the machine has become routine practice at the SNS. Nevertheless, we have not given up the idea of a model-based description of the beam dynamics in the linac.

This paper describes practical observations and the progress of our beam dynamics understanding since the last comprehensive overview that was presented at the HB2010 conference 13 years ago [4].

After descriptions of the linac, simulation models, and available diagnostics, the discussion will follow the classification suggested in [4]. We will talk about our success or failures in predictions and control of beam trajectories, longitudinal motion, bunch sizes and beam loss.

SNS LINAC

Different components of the SNS linac are shown in Fig. 1. All these components have different types of accelerating RF cavities. MEBT cavities are 1 RF gap cavities, and they perform longitudinal re-bunching of the beam after RFQ and matching longitudinal Twiss of the bunches to inject them into the DTL. The DTL and CCL have RF cavities with many RF gaps. The quadrupoles in the DTL cavities are permanent magnets, so transverse matching is performed in the MEBT section. The SCL has 97 RF cavities, and this is the most flexible section of the linac in terms of the cavity amplitudes and phases. The SNS linac produces 1 ms beam pulses with 38 mA peak current at 60 Hz repetition rate. Each 1 ms pulse is chopped into approximately 1000 mini pulses to provide a time structure for the ring injection. The chopping is performed before the entrance of the RFQ.

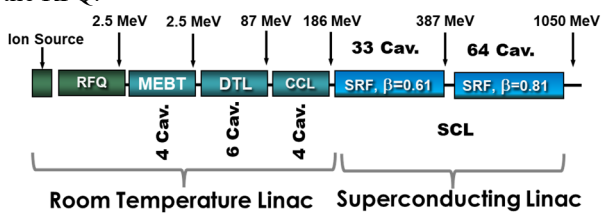

Figure 1: SNS linac.

LINAC SIMULATION CODES

Many linac simulation codes have been used at SNS during different stages of operation history, including PARMILA (the SNS was designed using this code), Trace3D, IMPACT3D, TRACK, XAL (or OpenXAL), and PyORBIT. Most of them were used in the early days of operations and power ramp-up. Lately, the most used code has been OpenXAL Online Model [5]. This code was developed initially at SNS and implements functionality similar to Trace3D, therefore it inherited all limitations of envelope simulation codes. For example, it cannot be used for beam loss calculations. The advantage of this type of code is its computational speed, which allows us to fit model parameters to real life data right in the control room. Combining this model with a graphical user interface (GUI) creates pow-

* This manuscript has been authored by UT-Battelle, LLC under Contract No. DE-AC05-00OR22725 with the U.S. Department of Energy. The United States Government retains and the publisher, by accepting the article for publication, acknowledges that the United States Government retains a non-exclusive, paid-up, irrevocable, worldwide license to publish or reproduce the published form of this manuscript, or allow others to do so, for United States Government purposes. The Department of Energy will provide public access to these results of federally sponsored research in accordance with the DOE Public Access Plan (http://energy.gov/downloads/doe-public-access-plan).
† shishlo@ornl.gov

ISBN: 978-3-95450-253-0 ISSN: 2673-5571 doi:10.18429/JACoW-HB2023-TUC2I2

erful interactive applications that can be used for linac tuning and beam dynamics experiments without offline analysis. Later, we will discuss two such applications that automated the SNS linac tune-up process.

The envelope codes simulate the transverse and longitudinal bunch sizes using only second order moments. This could be considered a big drawback, but in our experience, particle-in-cell (PIC) codes like PARMILA, IMPACT3D, and TRACK did not have a significant positive impact on the SNS operations. This is due to a lack of information about initial distributions, lattice imperfections, and imprecise knowledge of the RF system parameters during the early years of power ramp-up. Now we are accumulating more and more information about the initial particle distributions from the Beam Test Facility [6,7], and our accuracy of RF setting measurements is more precise. Therefore, our efforts to include PIC codes in our arsenal have been resurrected. We plan to use the PyORBIT code [8] for both offline and online analysis in the Python programming language environment.

BEAM DIAGNOSTICS

From the design stage of the SNS project, there was an intention to equip the accelerator with the full set of available at that time diagnostics. The SNS linac has following diagnostics devices:

- *Beam Position Monitors (BPM):* They are installed in all section of the linac after the RFQ. They measure and report to the control system the transverse beam center positions, its arrival time relative to the RF distribution line, and the amplitude of the second Fourier harmonic of BPM stripline signals. This amplitude is defined by the beam bunch longitudinal density distribution.
- Beam Current Monitors (BCM). Initially, they were installed in all sections of the warm linac, but in the DTL their signals were too noisy to be useful, and we lost all of them in the CCL section because the heat load on ceramic insertions caused cracking. The heat load was created by electron emission from the CCL RF cavities. Only two BCMs in the MEBT are used for peak current monitoring.
- Transverse Emittance Scanner (TES). We have a slit-harp (it can also work as a slit-slit) device in the MEBT and a laser wire emittance station right after the SCL.
- Bunch Shape Monitors (BSM). There are 4 BSMs in the CCL.
- Wire and Laser Wire Scanners (WS and LW). There are 5, 6, and 8 WSs in the MEBT, DTL, and CCL respectively. The SCL has 9 LW scanners for vertical and horizontal beam profile measurements.
- Beam Loss Monitors (BLM). There are 137 ionization chamber BLMs and 45 neutron detectors BLMs distributed along the linac.
- Faraday Cups (FC). There are 6 FCs in DTL, one after each DTL tank.

The BPMs, BLMs, LWs, and the laser wire emittance scanner are used during the SNS regular production time. All other diagnostic devices are used only in a low-power mode.

TRANSVERSE MOTION OF BEAM CENTER

The idealized approach to orbit correction includes measurements of transverse deviations of the beam using BPMs, calculating the necessary fields for dipole correctors using the lattice model, and applying these fields to the magnets to minimize the deviations. As reported in [4] we successfully used the OpenXAL Online Model for orbit correction in the MEBT, DTL, and CCL. For the CCL, we had to introduce significant and probably unphysical quadrupole offsets for a modified classical algorithm by including orbit zeroing for the whole section instead of only at BPM positions [4]. Nowadays, we first use the model-based orbit correction in the MEBT, then empirically tweak historic corrector settings in the DTL and CCL to reproduce the memorized BPM readings from the previous production run (those that gave us the lowest beam loss). We abandoned the modified trajectory correction algorithm in the CCL because the old quadrupole offset parameters do not work anymore. This could be due to changed RF settings (this will be discussed later) or the absence of possible non-zero transverse offset of the CCL RF cavities in the model. We did not study this subject further due to deficiencies in manpower, and because it did not affect beam loss, activation levels, or beam availability.

In the superconducting linac we successfully apply the classical orbit correction algorithm after applying the correct parameters of the RF system – amplitudes and phases of the SCL cavities.

Despite our problems with the orbit correction in the CCL, we have successfully benchmarked our Online Model against differential trajectory data in the DTL, CCL, and SCL. We measure the differential trajectory by changing one of dipole correctors and measuring the change of the horizontal and vertical beam positions at downstream BPMs. These changes are independent of any transverse offsets of any elements in the lattice. The average accuracy of the model is about 0.1 mm.

In the MEBT, our model is not accurate even for the differential trajectories, and to correct the orbit we have to use several iterations of the correction procedure. As we understand, this happens because of a hard-edge model of quadrupole fields in the OpenXAL OM. In Fig. 2 there are field gradients of several quadrupoles in the MEBT as functions of the position along the lattice. This picture demonstrates the importance of accounting for the distributed quad fields in MEBT beam dynamics simulations. To implement this type of the field in our model, we had to significantly modify the programming structure of the Java code in the OM.

ISBN: 978-3-95450-253-0 ISSN: 2673-5571 doi:10.18429/JACoW-HB2023-TUC2I2

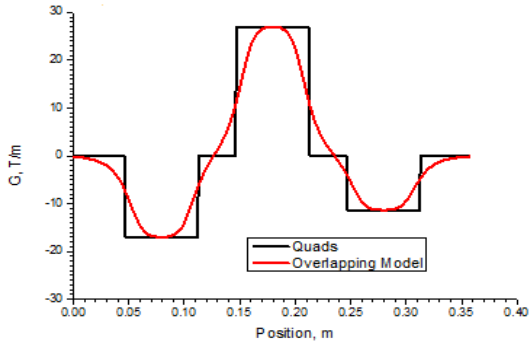

Figure 2: Field gradients of MEBT quadrupoles #5,6,7.

LONGITUDINAL MOTION OF BEAM CENTER

Our knowledge of the longitudinal motion of the bunch center was characterized in [4] as very good for all but the MEBT section. This conclusion still stands, but our method has significantly changed to allow automation of the tuning process, and its accuracy has greatly improved. From the beam dynamics point of view, the control of longitudinal motion means that we must set up RF cavities phases and amplitudes according to desirable values and calibrate our models for future use. The model parameters include RF parameters and the beam energy after each cavity. Each section in the linac has its own type of RF cavities, so we will discuss our procedures and results in subsections.

There are two common features of set-up procedures for all RF cavity types. First, during the set-up process, we do not scan the cavity amplitude. We only perform the cavity phase scan from -180^0 to +180^0 degree collecting downstream BPMs' phases. We found that this is faster and enough to find all parameters of the RF model. Second, we use short beam pulses (~ 1us) and an attenuator (metal grid mesh) right after RFQ which reduces the peak current by 80% to avoid beam loading effects in the RF cavities.

MEBT

Each RF cavity in MEBT has only one RF accelerating gap, so the set-up algorithm is very simple. These cavities do not accelerate the beam, so they should be set to 90^0 longitudinally focusing phase. After a 360^0 cavity phase scan, we perform a model-based fit of the BPM phases, which represent almost a sinusoid like curve. During the scan, all cavities downstream should not have any RF power, and the peak current and the pulse time length should be low enough to avoid any beam loading effects in them. After fitting, the model gives the correct phase for control system and the model amplitude of the cavity. Unfortunately, analysis with different BPMs still shows slightly different cavity phases than were reported in [4] (see Fig. 2 in [4]). An initial explanation of this phenomena blamed it on space-charge effects, but the effect did not disappear after 5 times peak current attenuation right after the RFQ exit. We believe this discrepancy is caused by the oversimplified model where we are using only one central particle instead of a longitudinally spread bunch with RMS around 20^0. Another reason could be asymmetrical distribution of the bunch in longitudinal phase space created by the RFQ. That just another argument to move to a PIC simulation code for analysis.

Nevertheless, the existing approach allows the operation group to restore the physical settings in the MEBT RF with accuracy acceptable for production.

DTL, CCL

The DTL and CCL have long multi-gap RF cavities. Originally implemented Phase Scan Signature (PSS) fitting and Delta-T methods for RF cavity setup that used the BPM in the next downstream cavity were replaced by PSS with the BPM inside the tuned-up cavity. In this case we are tuning only part of the cavity between the entrance and this BPM, but it is the equivalent of tuning up the whole cavity if the model correctly reproduces the cavity design. Figure 3 describes the measurement scheme.

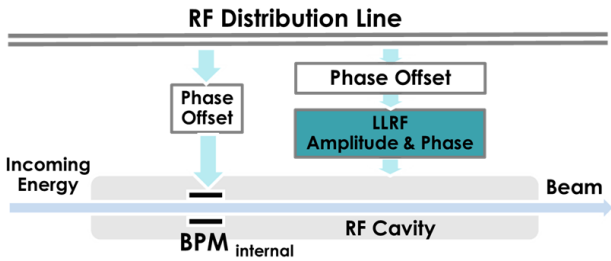

Figure 3: DTL and CCL phase scan with inner BPM.

The cavity phase scan also performed in 360^0 phase range at the existing RF amplitude. The position of BPM should be close enough to the beginning of the cavity to provide good beam transmission and bunching for strong signals from this BPM, and it should be far away enough from the beginning (several RF gaps) to give non-sinusoidal BPM phase response during the scan.

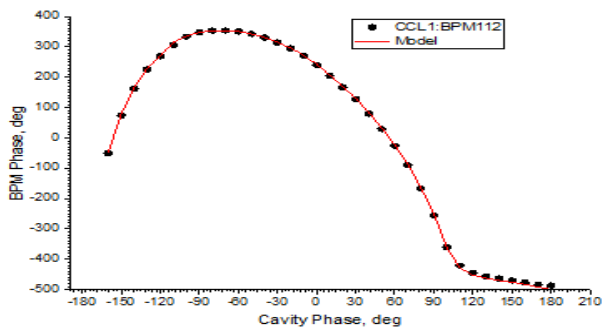

Figure 4: CCL1 phase scan with inner BPM.

Figure 4 shows the result of the phase scan cavity CCL1. There are 12 accelerating RF gaps between the BPM112 and the CCL1 entrance. The obvious non-sinusoidal shape of the curve allows to find not only the cavity's amplitude and phase, but also, we got the entrance beam energy after fitting procedure. The accuracy of the fitted model beam energy for case shown in Fig. 4 was 21 keV for the found energy 86.897 MeV. The design energy is 86.828 MeV.

ISBN: 978-3-95450-253-0 ISSN: 2673-5571 doi:10.18429/JACoW-HB2023-TUC2I2

SCL

Each RF cavity in the SCL has only 6 accelerating gaps, so a 360^0 phase scan gives the sin-like functions for the phases of all downstream BPMs. All cavities downstream of the scanned one should not have the RF field in them during the beam presence. This state of the cavities we call "blanked", and we "blank" only 1 RF pulse out of 60 for every second to keep the heat load of superconducting cavities approximately stable. Initially, we used the scan data from only two BPMs for the model-based fitting. This pair of BPMs had to be time-calibrated to measure the beam energy by using the time-of-flight approach. Later, we developed algorithm to include all available BPMs in analysis. The time calibration for all BPMs is performed by using the final beam energy measured in the SNS ring [9].

The procedures of the phase scans of all cavities in SCL and the data analysis have been automated, and the whole process now take about 45 minutes for all 97 cavities. The analysis produces a calibrated model of the SCL linac which can be used to quickly rescale the cavity phases in case one or two of them fail. Rescaling is also performed when the field gradients of some cavities must be reduced to mitigate an elevated trip rate [10].

Design Parameters and Empirical Tuning

The tuning procedures described in this section have allow us to scan the existing state of the machine, to save the physical RF parameters (the phase of the fist RF gap at the moment of bunch arrival and the field gradient of cavities) of this state, and the quickly restore this state even after RF distribution line repair. The SNS Operations Group have used this functionality to perform empirical tuning of the RF system (phases and amplitudes) to lower beam loss and cavity trip rates throughout the linac. This tuning was performed during several high-power production runs, and it resulted in cavity phases and amplitudes significantly different from design parameters.

Table 1: CCL Linac RF System Parameters

Cavity	Design φ_{synch}, deg	A/A_{design} %	Production φ_{synch}, deg
CCL1	-30.9	93	-16.7
CCL2	-30.8	95	-21.6
CCL3	-30.7	98	-23.9
CCL4	-29.3	93	-18.3

As an example, the production and design parameters of the CCL cavities are shown in Table 1. Despite significant deviation from the design values, the tuned parameters give low beam loss/activation, low trip rate of RF cavities, and the stable high-power linac operation. This situation was discussed in [11]. It was concluded that there no contradiction to classical beam dynamics simulation models for linacs.

TRANSVERSE PROFILES OF BEAM AND RMS SIZES

There has not been much progress on transverse beam size control in the SNS linac since the HB2010 report [4]. Several attempts to create matched beams in the DTL, CCL, and SCL using the OpexXAL Online Model or PIC codes failed to reduce beam loss. Eventually, the satisfactory beam loss was achieved by empirical tweaking quadrupoles gradients around the design values in the MEBT, DTL, and CCL. In the SCL, the quad fields were changed significantly, as described in the Introduction section. As a result of all deviations from the design, the transverse rms emittances at the SCL exit are 2.5 and 1.5 times bigger than the design value for horizontal and vertical directions respectively. The emittances measured by Laser Wire stations right downstream of SCL are shown in Fig. 5. We believe that we have reached an equilibrium between decreasing beam loss (induced by IBSt [3]) with the bigger transverse sizes and increasing loss on the beam pipe apertures. It is possible that we have only found a local beam loss minima, and we plan to study this subject further.

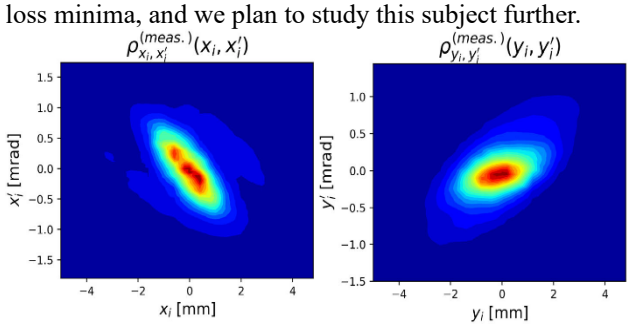

Figure 5: Horizontal and vertical transverse phase spaces after SCL.

Figure 5 demonstrates significant S-shaped shoulders for the horizontal plane and different Twiss parameters of the core and periphery for the vertical plane. Such phase space distributions cannot be described with rms sizes only. For us it is just another argument to add PIC simulation codes to our arsenal of models.

LONGITUDINAL BUNCH SIZES

The SNS has historically had two types of diagnostics to measure the bunch longitudinal distribution and its rms length. The first one was Bunch Shape Monitors in CCL, and the second one was a Faraday Cup after the DTL1 tank which can be used to extract the rms from the beam transmission curve after the phase scan of this tank. Later, we created other methods to measure and to use the longitudinal bunch sizes in the SNS linac.

RMS Bunch Length in SCL

First, we developed a method to measure longitudinal rms of bunch sizes in SCL by analysis the BPMs' amplitudes as a function of the RF cavity phase during the phase scan [12]. We used the fact that the amplitude of BPM signal depends on the bunch size:

ISBN: 978-3-95450-253-0 ISSN: 2673-5571 doi:10.18429/JACoW-HB2023-TUC2I2

$$I(\sigma) = I_{peak} \cdot \exp\left(-\frac{\sigma^2}{2}\right) \quad (1)$$

where σ is a rms bunch length in radians at the BPM's frequency. By changing the cavity phase, we are changing longitudinal focusing-defocusing of the bunch. If the BPM is far enough from the cavity, the variation of the BPM amplitude can be used to extract the longitudinal Twiss parameters of the beam at the cavity entrance. This is similar to an analysis of wire scanner data during a quadrupole field gradient scan to get transverse Twiss parameters of the beam. The peak current parameter in Eq. (1) is the BPM amplitude during the production, because the rms bunch sizes in production are very small 2-3^0, and the exponent in this equation is equal to 1. Figure 6 shows the results of the phase scan of the first cavity in the SCL. The curves at the top of the picture belong to BPMs closest to the cavity. These curves are practically constant, because there is not enough distance for noticeable bunching/de-bunching development. Only data from BPMs far enough from the cavity show the clear signature and can be used for analysis.

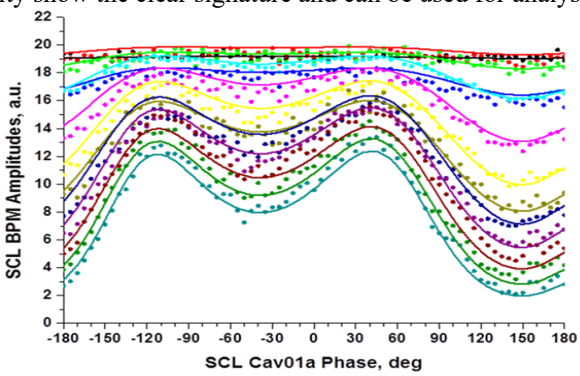

Figure 6: BPM amplitudes as functions of the first SCL cavity phase.

This method has limitations. For the SNS superconducting linac we can use it only for the medium-beta section (see Fig. 1), because for higher energies we do not have enough distances between the cavity of interest and downstream BPMs. Also, we must have ability to get the peak current parameter in Eq. (1) by getting the BPM signal for a very short bunch which we can easily do in SCL.

RMS Bunch Length in MEBT

In the MEBT we cannot create short enough bunches to calibrate BPM amplitudes. The RF cavities are not strong enough for this task. Nevertheless, it was shown that using two cavities with known parameters and one BPM we can simultaneously extract the longitudinal Twiss parameters of the beam and calibrate BPM amplitude in Eq. (1) using data from the phase scans of these two cavities [13]. Figure 7 demonstrates a good agreement between the bunch length at the DL1 entrance measured by a classical DTL1 acceptance scan with the Faraday Cup and the simulations with the longitudinal Twiss parameters found by the described above method. The bunch lengths were measured for different voltages of the MEBT last buncher cavity.

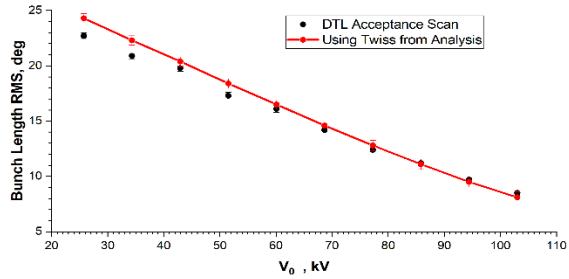

Figure 7: Bunch length vs. voltage of last MEBT buncher.

BEAM LOSS AND RF PHASE STABILITY IN SCL

In the subsection "Design Parameters and Empirical Tuning" we discussed the acceptable (from the high-power operations point of view) differences between the design and production RF system parameters for the SNS warm linac. For the SCL there are no exact design RF parameters since the commissioning time. The amplitudes of the cavities had and have wide variation, and they are defined by the RF group. These amplitudes should be maximal to reach the design value of the final linac energy. On the other hand, they should be low enough to provide stable operation of each cavity. The phases of the cavities are found after a long empirical tuning process started around –(15÷18) deg. synchronous phase. We have more freedom in choosing these phases for the cavities at the end of linac, so we keep one or two cavities at the end of SCL without beam acceleration. This allows us to correct the final energy after rescaling of the SCL.

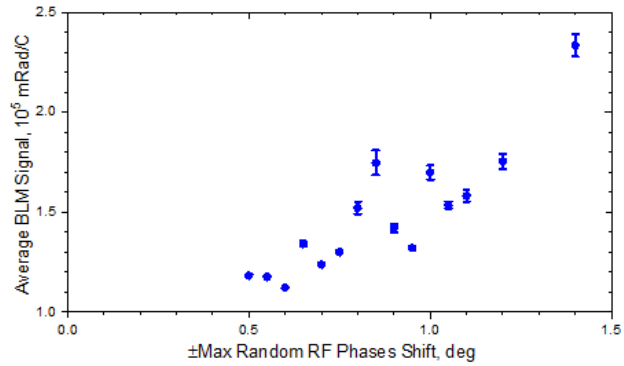

Figure 8: Average beam loss in SCL as function of random RF phase limit.

The interesting question for us was an acceptable accuracy of the RF settings for the SCL. We performed an experiment using operation-like settings. In this experiment we measured the average beam loss in the SCL for a set of 100 random RF settings around existing production values. The set different maximal uniform random deviations for the phases and collected average beam loss as a function of these maximal values. The results are shown in Fig. 8. We did not see any noticeable changes of beam loss if the phase changed less than 0.5^0, so the plot in Fig. 8 starts at this point. These results tell us that random variations of the RF phases in the SCL less than 1^0 do not create unacceptable beam loss for our linac. And we should keep in mind that

ISBN: 978-3-95450-253-0 ISSN: 2673-5571 doi:10.18429/JACoW-HB2023-TUC2I2

this limit of 1^0 was found for a very imperfect beam condition. First, the transverse beam sizes were blown up (see the section with transverse beam sizes), and second, the bunch phases measured by BPMs are different along the 1 ms beam pulse. For production conditions this phase difference between bunches at the head and the tail could be ~5^0. For superconducting linacs with protons, blown up of the rms transverse sizes should not be a problem and the 1^0 limit for RF phase noise will be much higher.

CONCLUSION

Most of our knowledge and understanding of the SNS linac beam dynamics has come from the Open XAL Online model, an envelope code that can simulate the dynamics of single particle motion and the rms sizes of the bunch. Using this tool, we have successfully characterized the physical parameters of the RF system. We can restore these parameters, recalculate the cavity phases in the superconducting linac in the case of failure of one or two cavities, and control the beam trajectory throughout the linac. One of drawbacks of this tool is its inability to predict beam loss not related to the intra-beam stripping mechanism.

We can also measure the transverse and longitudinal bunch sizes, profiles, and phase space distributions using our advanced beam instrumentation devices. Unfortunately, we do not know how to translate this knowledge into bean loss reduction or improved operational practices. We think we can make a progress in this direction by adding realistic PIC simulation codes to our online model. Although this approach failed before, we now have a better understanding of the longitudinal settings of our lattice from the Online Model and of the initial particle distribution in 6D phase space from the Beam Test Facility.

ACKNOWLEDGEMENTS

The author thanks the members of the SNS Beam Instrumentation and Accelerator Physics groups and SNS Operations for many years of fruitful collaboration, help, and useful discussions.

REFERENCES

[1] S. Henderson *et al.*, "The Spallation Neutron Source accelerator system design", *Nucl. Instrum. Methods Phys. Res., Sect. A*, vol. 763, pp. 610-673, 2014. doi:10.1016/j.nima.2014.03.067

[2] J. Galambos, "SNS High Power Operation - Expectations and Experience", in *Proc. HB'10*, Morschach, Switzerland, Sep.-Oct. 2010, paper MOIB01, pp. 11-15.

[3] A. Shishlo *et al*., "First observation of intra-beam stripping of negative hydrogen in a superconducting linear accelerator," *Phys. Rev. Lett.,* vol. 108, p. 114801, June 2012. doi:10.1103/PhysRevLett.108.114801

[4] A. V. Aleksandrov, "Challenges of Reconciling Theoretical and Measured Beam Parameters at the SNS Accelerator Facility.", in *Proc. HB'10*, Morschach, Switzerland, Sep.-Oct. 2010, paper WEO2D01, pp. 539.

[5] A. P. Zhukov *et al.*, "Open XAL Status Report 2022", in *Proc. IPAC'22*, Bangkok, Thailand, Jun. 2022, pp. 1271-1274. doi:10.18429/JACoW-IPAC2022-TUPOTK029

[6] Z. Zhang *et al*., "Design and commissioning of the beam test facility at the spallation neutron source", *Nucl. Instrum. Methods Phys. Res., Sect. A*, vol. 949, p. 162826, 2020. doi:/10.1016/j.nima.2019.162826

[7] A. Hoover *et al*., "Analysis of a hadron beam in five-dimensional phase space," *Phys. Rev. Accel. Beam,* vol. 26, p. 064202, 2023. doi:10.1103/PhysRevAccelBeams.26.064202

[8] A. P. Shishlo, "Linac Beam Dynamics Simulations with PyORBIT", in *Proc. ICAP'12*, Rostock-Warnemunde, Germany, Aug. 2012, paper MOSBC2, pp. 20-22.

[9] J. C. Wong *et al*., "Laser-assisted charge exchange as an atomic yardstick for proton beam energy measurement and phase probe calibration," *Phys. Rev. Accel. Beams*, vol. 24, p. 032801, 2021. doi:10.1103/PhysRevAccelBeams.24.032801

[10] V. S. Morozov, C. C. Peters, A. P. Shishlo, "Oak Ridge Spallation Neutron Source superconducting rf linac availability performance and demonstration of operation restoration with superconducting rf cavity off," *Phys. Rev. Accel. Beams,* vol. 25, p. 020101, 2022. doi:10.1103/PhysRevAccelBeams.25.020101

[11] A. Shishlo, C. Peters, "Comparison of design and production RF settings at SNS normal temperature linac," in *Proc. IPAC'23*, Venice, Italy, 7-12 May 2023, pp. 2219-2222. doi:10.18429/JACoW-IPAC2023-TUPM015

[12] A. Shishlo, A. Aleksandrov, "Non-Interceptive method to measure longitudinal Twiss parameters of a beam in a hadron linear accelerator using beam position monitors,". *Phys. Rev. Spec. Top. Accel Beams*, vol. 16, p. 062801, 2013. doi:10.1103/PhysRevSTAB.16.062801

[13] A. Shishlo, A. Aleksandrov, "Measuring longitudinal beam parameters in the low energy section of the Oak Ridge Spallation Neutron Source accelerator," *Phys. Rev. Accel. Beams*, vol. 21, p. 092803, 2018. doi:10.1103/PhysRevAccelBeams.21.092803